J. Fluid Mech. (2002), *vol.* 459, *pp.* 307–316.
DOI: 10.1017/S0022112002008406 Printed in the United Kingdom

Flux Richardson number measurements in stable atmospheric shear flows

By E. R. PARDYJAK[1], P. MONTI[2] AND H. J. S. FERNANDO[2]

[1]Department of Mechanical Engineering, University of Utah, Salt Lake City, UT 84112, USA

[2]Environmental Fluid Dynamics Program, Department of Mechanical and Aerospace Engineering, Arizona State University, Tempe, AZ 85287-9809, USA

(Received 28 September 2001 and in revised form 20 February 2002)

The flux Richardson number R_f (also known as the mixing efficiency) for the stably stratified atmospheric boundary layer is investigated as a function of the gradient Richardson number Ri_g using data taken during two field studies: the Vertical Transport and Mixing Experiment (VTMX) in Salt Lake City, Utah (October 2000), and a long-term rural field data set from Technical Area 6 (TA-6) at Los Alamos National Laboratory, New Mexico. The results show the existence of a maximum R_f (0.4–0.5) at a gradient Richardson number of approximately unity. These large-Reynolds-number results agree well with recent laboratory stratified shear layer measurements, but are at odds with some commonly used R_f parameterizations, particularly under high-Ri_g conditions. The observed variations in buoyancy flux and turbulent kinetic energy production are consistent with the concept of global intermittency of the atmospheric stable boundary layer.

1. Introduction

The flux Richardson number,

$$R_f = \frac{-\overline{b'w'}}{-\overline{u_i'u_j'}(\mathrm{d}\bar{U}_i/\mathrm{d}x_j)}, \tag{1.1}$$

is a key parameter in modelling oceanic and atmospheric flows. It expresses the ratio of the buoyancy flux ($\overline{b'w'}$) and the production of turbulent kinetic energy (TKE) $-\overline{u_i'u_j'}(\partial\bar{U}_i/\partial x_j)$ in the TKE equation, which takes the form (Mellor & Yamada 1982)

$$\frac{\partial q^2/2}{\partial t} + \bar{U}_j\frac{\partial q^2/2}{\partial x_j} = \overline{u_i'u_j'}\frac{\partial\bar{U}_i}{\partial x_j} + \frac{\partial M_j}{\partial x_j} + \overline{b'w'} - \epsilon, \tag{1.2}$$

where b' is the buoyancy fluctuation, $u_i' = (u', v', w')$ are velocity fluctuations with w' anti-parallel to the gravitational acceleration g (in the z-direction), $q^2/2$ the TKE, ϵ the TKE dissipation rate, $\partial M_j/\partial x_j$ the energy flux divergence and $\bar{U}_j(\partial(q^2/2)/\partial x_j)$ the advection of TKE. In stably stratified flows $\overline{b'w'} < 0$ represents the destruction of local density gradients to produce a vertical mass flux (known as stirring). The buoyancy fluctuations associated with stirring dissipate at molecular scales, causing irreversible destruction of the buoyancy gradient (mixing). Although (1.1) does not rigorously represent mixing, it is often referred to as the mixing efficiency (Ivey & Imberger 1991; Caulfield & Peltier 2000).

The flux Richardson number is directly related to the eddy diffusivities of buoyancy

k_b and momentum k_m, and hence is a key parameter in geophysical modelling. Note that for a parallel shear flow with $\bar{U} = \bar{U}(z)$, $k_b = -\overline{b'w'}/N^2$ and $k_m = -\overline{u'w'}/\mathrm{d}\bar{U}/\mathrm{d}z$, the flux Richardson number can be written as $(k_b/k_m) = (R_f/Ri_g)$, where

$$Ri_g = N^2/(\mathrm{d}\bar{U}/\mathrm{d}z)^2 \tag{1.3}$$

is the gradient Richardson number, $N = [(-g/\rho_0)(\partial\bar{\rho}/\partial z)]^{1/2}$ the buoyancy (or Brunt–Väisälä) frequency, $\bar{\rho}$ the mean density and ρ_0 a reference density. If the flow is stationary and homogeneous (i.e. uniform shear), (1.2) simply becomes a balance between the production and dissipation of TKE, and buoyancy flux. This balance is expected to hold approximately in an integral form, when the integral is taken over a suitable section where there is negligible energy diffusion across boundaries, the flow is stationary and the energy accumulation due to advection is insignificant, for example, as assumed in the Osborn (1980) model for the evaluation of oceanic k_b. In this case, (1.1) and (1.2) give

$$k_b = \frac{R_f}{(1-R_f)}\frac{\epsilon}{N^2} = \Gamma\frac{\epsilon}{N^2}, \tag{1.4}$$

where Γ is called the 'mixing' (or 'flux') coefficient (Oakey 1982). To date, a general expression for R_f has not been established, and various empirical expressions are used for Γ. For example, Osborn (1980) assumed $R_f \leqslant 0.15$ ($\Gamma \leqslant 0.2$) for oceans whereas values of $\Gamma \approx 0.33$ (Lilly, Waco & Adelfang 1974) and $\Gamma \approx 0.8$ (Weinstock 1978) have been proposed for the upper atmosphere on theoretical grounds. Indirect estimates by Oakey (1982) using oceanic measurements show wide variability for Γ, 0.259 ± 0.21, indicating that Γ (or R_f) is highly variable. This variability supports the available theories of fine structure evolution in oceans (Phillips 1972) and the atmosphere (Posmentier 1977).

The flux Richardson number is a key quantity embedded in turbulence modelling of geophysical flows. For example, the relationship between R_f and Ri_g is used in the Mellor & Yamada (1982, hereafter MY82) and Nakanishi (2001) closure schemes. By solving a set of simplified equations for the Reynolds stresses and heat flux, Yamada (1975) and MY82 proposed

$$R_f = 0.725[Ri_g + 0.186 - (Ri_g^2 - 0.316Ri_g + 0.0346)^{1/2}], \tag{1.5}$$

which yields a maximum flux Richardson number of 0.25. Nakanishi (2001) used LES for non-neutral periods to improve the MY82 parameterization,

$$R_f = 0.774[Ri_g + 0.220 - (Ri_g^2 - 0.328Ri_g + 0.0484)^{1/2}]. \tag{1.6}$$

Earlier attempts to theoretically determine R_f include that of Townsend (1958), which was directed at determining the requisites for sustained turbulence in atmospherically stably stratified flows. Simplified equations for TKE and temperature fluctuations, excluding radiative effects were used to derive

$$R_f = \tfrac{1}{2}[1 - (1 - 12\eta Ri_g)^{1/2}] = \tfrac{1}{2}[1 - (1 - Ri_g/Ri_{g,cr})^{1/2}], \tag{1.7}$$

where $\eta = L_\theta/L_\epsilon(k_\theta/k_u)^2$, L_ϵ and L_θ are the dissipation length scales for TKE and temperature fluctuations, $k_u = |\overline{u'w'}|/\overline{w'^2}$ and $k_\theta = |\overline{w'\theta'}|/(\overline{w'^2}\cdot\overline{\theta'^2})^{1/2}$. Here $Ri_{g,cr}$ is a critical gradient Richardson number beyond which turbulence is extinguished. Townsend assumed $\eta \sim 1$ for all conditions, yielding $Ri_{g,cr} = 1/12$ and a maximum $R_f = 0.5$ (also see Caulfield & Kerswell 2001).

Most meso-scale atmospheric codes utilize parameterizations such as (1.5)–(1.7) for

closure, and these codes are known to perform poorly under stable conditions. Therefore, it is of interest to verify R_f–Ri_g relationships used in common closure models. Most of the available R_f–Ri_g data have been obtained in the laboratory (mainly using indirect methods), with the results presented as functions of parameters other than Ri_g (Linden 1980; McEwan 1983). Direct measurements of R_f in laboratory experiments (Strang & Fernando 2001*a*, *b*; hereafter SF01*a*, *b*) and direct numerical simulations (Caulfield & Peltier 2000) of stratified shear layers have been reported recently, but at relatively low Reynolds numbers. In the present work, direct measurements of R_f are presented over a range of Ri_g in high-Reynolds-number, naturally occurring stratified shear flows.

The type of stratified shear flow considered here is the downslope (katabatic) flow occurring along inclined surfaces at night as a result of radiative cooling of the Earth's surface. Since this is one of many types of shear flows possible in nature, a question arises regarding the general applicability of results obtained from such flows, for example, for flat-terrain atmospheric boundary layers. Most natural flows can be considered to be in local equilibrium at scales smaller than the scale of flow inhomogeneities, and hence their small-scale properties are expected to depend on local variables. As pointed out by Nieuwstadt (1984) and Sorbjan (1986), the flat-terrain atmospheric boundary layer is in local equilibrium and characterized by z/L (where L is the Monin–Obukhov scale) or Ri_g. A similar conclusion is also possible for natural slope flows (Mahrt 1982). More to the point, in environmental flows, N and $\mathrm{d}\bar{U}/\mathrm{d}z$ are not uniform, and their variation occurs over the scales $L_N = (\partial\bar{\rho}/\partial z)/(\partial^2\bar{\rho}/\partial z^2)$ and $L_v = (\partial\bar{U}/\partial z)/(\partial^2\bar{U}/\partial z^2)$, respectively. These scales are typically large compared to the buoyancy length scale $L_b = \sigma_w/N$ and the shear length scale $L_S = \sigma_w/(\mathrm{d}\bar{U}/\mathrm{d}z)$ of stratified turbulence, where σ_w is the r.m.s. vertical velocity. These represent, respectively, the length scales where buoyancy and shear play important roles. For the drainage flows considered here, typical values are $L_N = 10\,\mathrm{m}$, $L_v = 50\,\mathrm{m}$, $L_b = 4\,\mathrm{m}$ and $L_S = 3.7\,\mathrm{m}$ (for $\sigma_w = 0.2\,\mathrm{m\,s^{-1}}$, $\mathrm{d}\bar{U}/\mathrm{d}z = 0.054\,\mathrm{s^{-1}}$ and $N = 0.05\,\mathrm{rad\,s^{-1}}$). Therefore, the small-scale turbulence dynamics are expected to be shielded from larger scale inhomogeneities. In addition, the global internal wave field is expected to have negligible influence on local dynamics. Such flows can be studied under the guise of homogeneous stratified shear flows, and can be compared with kindred laboratory flows. Two limits can be considered:

(i) $L_b > L_S$ or $Ri_g^{1/2} < 1$: In this case, weak stratification allows large vertical displacement of fluid parcels over distances larger than the scale where straining of the mean shear is felt by the eddies. Continuous feeding of TKE from the mean shear to turbulence is expected, thus sustaining turbulence and mixing.

(ii) $L_b < L_S$ or $Ri_g^{1/2} > 1$: The turbulent motions in this case are confined to scales smaller than those affected by shear, and hence, weak interaction between mean shear and turbulence is expected. Turbulence in this case is sporadically generated, patchy in space and is expected to decay rapidly.

If the buoyancy flux and shear production are parameterized as follows: $-\overline{b'w'} = c_b N^2(\sigma_w/N)\sigma_w$ and $-\overline{u'w'}(\mathrm{d}\bar{U}/\mathrm{d}z) = c_u\sigma_w\sigma_u(\mathrm{d}\bar{U}/\mathrm{d}z)$, respectively, where c_b and c_u are correlation coefficients, then

$$R_f \approx \left(\frac{c_b}{c_u}\right) Ri_g^{1/2} \left(\frac{\sigma_w}{\sigma_u}\right). \tag{1.8}$$

For case (i) with sustained turbulence $Ri_g \ll 1$, c_b and c_u can be assumed to be independent of Ri_g and $\sigma_u \sim \sigma_w$, yielding $R_f \sim Ri_g^{1/2}$ (e.g. Stretch, Nomura &

Rottman 2000). For $Ri_g \gg 1$, however, σ_w/σ_u, c_b and c_u are all Ri_g dependent, causing R_f to decrease with Ri_g (Ivey & Imberger 1991). On the other hand, in atmospheric studies $R_f \sim Ri_g$ is often used by assuming $k_b/k_m \approx$ constant for low stabilities in the expression $(k_b/k_m) = (R_f/Ri_g)$.

The aim of this paper is three-fold: first, to present Ri_g data obtained in high-Reynolds-number natural turbulent flows and verify whether the laboratory data of SF01*a*, *b* are representative of natural stratified shear flows. Second, to evaluate certain available parameterizations for R_f such as those proposed by Townsend (1958), MY82 and Nakanishi (2001), and third, to use flux measurements made during the study to identify global intermittency in atmospheric nocturnal flows.

Two sets of atmospheric katabatic flow data taken at different localities and under nocturnal stable conditions were used for this study. One field data set is based on a long-term rural tower in Los Alamos, New Mexico, and the other was obtained during the Vertical Transport and Mixing Experiment (VTMX) conducted in Salt Lake City, Utah. With the stratification slowly changing over the night, a wide range of stability conditions spanning two decades of Ri_g variation were realized. The changes were slow and the flow evolution could be considered as occurring via a series of quasi-stationary steps (over a carefully selected averaging period).

2. The experiments

2.1. *Los Alamos TA-6 data*

The rural field data were obtained from the Los Alamos National Laboratory's 92 m, Technical Area 6 (TA-6) meteorological tower (latitude: north 35.964, longitude: west 106.340), as part of a long-term meteorological data set. The site is located within a high desert (2260 m above sea level) Ponderosa pine forest on the Pajarito Plateau. The slope of the plateau is approximately 0.03 rising to the west-northwest with very steep slopes (> 0.15) approximately 6.5 km up slope (to the northwest). There are several hundred metres of fetch directly surrounding the tower composed mostly of grass and small shrubs (aerodynamic roughness length, $z_0 \approx 0.1$ m).

This data set covers thousands of 900 s averages over the period April 1999–October 2000. Only precipitation-free nights between April and October were used. The sensible heat and momentum fluxes were calculated from the data obtained at 12 m above the ground using an ATI (Applied Technologies, Inc.) three-component Sx-type sonic anemometer. The data were sampled at 10 Hz; see Baars, Hott & Stone (1998) for more details of the site and measurements. The resolution for the wind speed and temperature was 0.01 m s^{-1} and 0.01 °C, respectively, with a wind speed measurement accuracy of ± 0.05 m s^{-1} and sonic temperature accuracy of ± 0.05 °C. To calculate the gradient and flux Richardson numbers, mean gradients of both temperature and wind speed are needed. Temperature gradients were obtained using a standard central differencing scheme. The individual temperature data were measured at 1.2, 12 and 23 m. In addition, the wind speeds were measured at 12, 23 and 46 m above the ground (non-uniformly spaced). The lowest wind measurement was at 12 m which coincided with the location of turbulence measurements. Since the next two available wind speed measurements were above this point, a one-sided differentiating scheme was necessary. The differentiation was accomplished using a finite difference formula for arbitrarily spaced grids (see Fornberg 1996, pp. 167–169).

The buoyancy frequency was calculated using $N = ((g\,\partial\bar{\theta}_v/\partial z)/\Theta_v)^{1/2}$ where $\bar{\theta}_v$ is the mean virtual potential temperature and Θ_v is a reference value. The gradient

Richardson number was calculated using (1.3). The flux Richardson number can be evaluated, neglecting subsidence, using (1.1) as $R_f = (g/\Theta_v)\overline{w'\theta_v'}/(\overline{u'w'}\,\mathrm{d}\bar{U}/\mathrm{d}z)$, where θ_v' is the fluctuating virtual potential temperature. Since fluctuations of air humidity and pressure were not routinely measured, potential temperature instead of virtual potential temperature was utilized for the calculations. Owing to the relative dry conditions that prevailed during the measurements, the resulting error was estimated to be less than 5%.

2.2. *VTMX field experimental data from Salt Lake City*

The Salt Lake City metropolitan area lies in a valley located at $\sim$ 1400 m above sea level. The valley is approximately 30 km wide (east-west) and 50 km long (north-south) and is surrounded by mountains ($>$ 3000 m). The northwesterly border of the valley coincides with the southern shoreline of the Great Salt Lake.

The observation site, located in the north-easterly part of the valley, consisted of a grassy area ($z_0 \approx 0.1$ m) in the proximity of the Mont Olivet Cemetery (latitude: north 40.753, longitude: west 111.849). This area had a slope of 0.07 and was void of buildings and trees within about 100 m.

The meteorological measurement equipment consisted of a 14.0 m tower equipped with two cup anemometers mounted at 2.0 m and 7.3 m levels, two thermistors placed at 1.8 m and 6.9 m, and sensors measuring downward and upward radiation at 3.0 m. A data logger provided storage of 5 min averages of air temperature, wind speed and solar radiation. Two ultrasonic fast response (10 Hz sampling rate) anemometer–thermometers were placed at 4.5 m (ATI Sx-type) and 13.86 m (Metek GmbH. Resolution: wind speed 0.01 m s^{-1}, temperature 0.01 °C). This suite of instruments provided capabilities of heat and momentum flux measurements averaged over a desired time interval. Time series acquired from 17:00 to 07:00 LST (local standard time) from October 1 to October 5, 2000 by the two sonic anemometer–thermometers were used to evaluate Richardson numbers. The momentum and heat fluxes corresponding to the upper probe were used for the calculations, but the fluxes did not differ between the two probes by more than $\pm$10%. The vertical distance 9.36 m between the two sonic anemometers was used for discrete differencing to obtain velocity shear. Note that the assumed linear profile can introduce an error in the Ri_g. However, given $L_N = 10$ m and $L_v = 50$ m, the error is expected to be small $<$ 10%, which was estimated on the basis of differences obtained using linear and logarithmic velocity profiles. Further, because of the presence of internal waves in the flow, Ri_g can fluctuate rapidly. This can be captured only if the measurement resolution exceeds the Ozmidov length scale (DeSilva *et al.* 1999). Estimates indicate that this requirement was not strictly satisfied, resulting in an error margin of $\pm$10% due to inadequate spatial resolution. A detailed discussion of this is given in Monti *et al.* (2002).

Given the variability of natural motions, it was necessary to ensure that the averaging performed was capable of capturing turbulent phenomena in a katabatic flow. To this end, VTMX data were subjected to a thorough analysis, where R_f–Ri_g curves were calculated with averaging periods varying from 30 s to 1800 s in increments of 15 s. The data consistently showed that the R_f–Ri_g curves are insensitive to averaging times of 60 s to 900 s. This period encompassed several eddy turnover times of the stratified turbulence in point, which has a time scale on the order of $N^{-1} \sim 20$ s. The averaging time used covers the shear time scale $|\mathrm{d}\bar{U}/\mathrm{d}z|^{-1} \sim 1$ s but not the natural variability (e.g. front arrival, oscillations due to global intermittency shown in figure 3) of the flow ($\sim$ 1 hour).

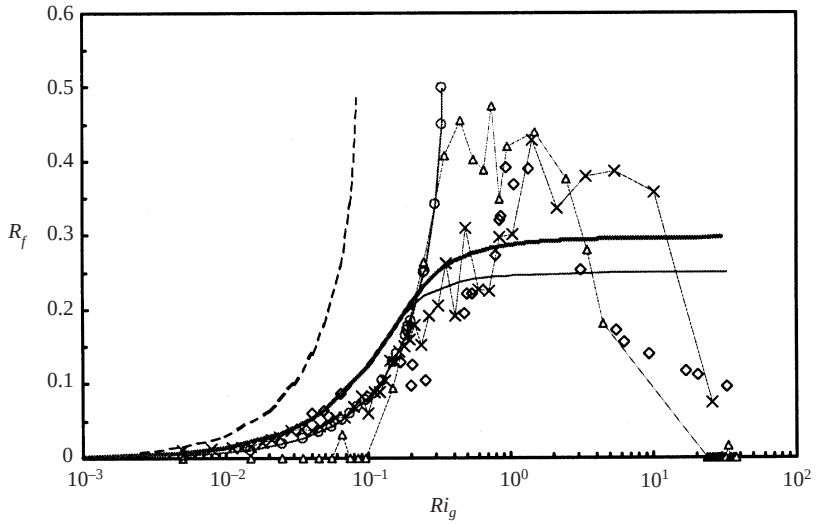

FIGURE 1. Mixing efficiency (R_f) as a function of gradient Richardson number (Ri_g): – – – – –, Townsend (1958); ——, Mellor & Yamada (1982); ——, Nakanishi (2001); —△—, VTMX; —×—, TA-6; ◇, Strang & Fernando (2001*b*); —○—, Townsend with $\eta = 1/4$.

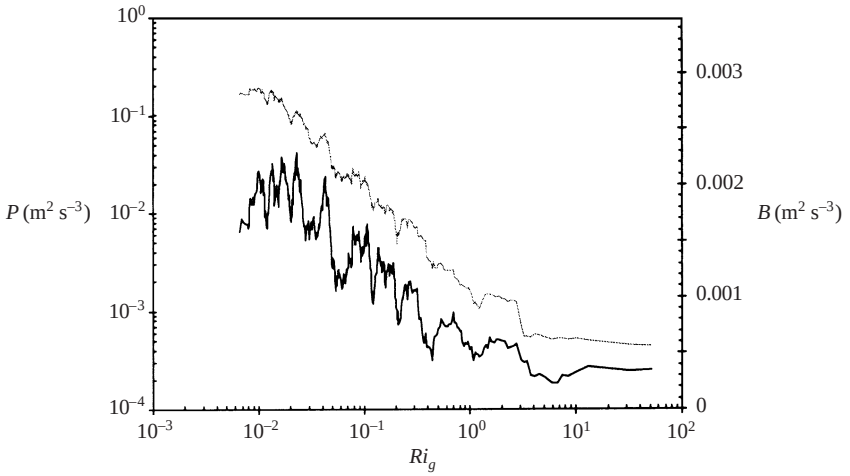

FIGURE 2. The variation of shear production (P: ——) and buoyancy flux (B: ——) with the gradient Richardson number (Ri_g). 900 s averaged nocturnal boundary layer data taken from the TA-6 site over two weeks are shown.

3. Results and discussion

Figure 1 is a plot of flux Richardson number versus gradient Richardson number for the two sets of field data (averaged over 900 s) and the laboratory data of SF01b. The parameterizations of MY82, Townsend and Nakanishi are also shown ((1.5)–(1.7)). (Note that the VTMX data contain multiple points where the $R_f = 0$. This was an artifact that resulted from a lack of data during these periods.) The details of the curves (e.g. rates of increase or decrease) differ for each site, which may be attributed to a variety of reasons, including the sensitivity of R_f to the flow details (e.g. profiles) and contributions of non-local processes. All three data sets, however, show the same general trend: a slow increase of R_f for $Ri_g < 0.1$, a steep increase for $0.1 < Ri_g < 1.0$,

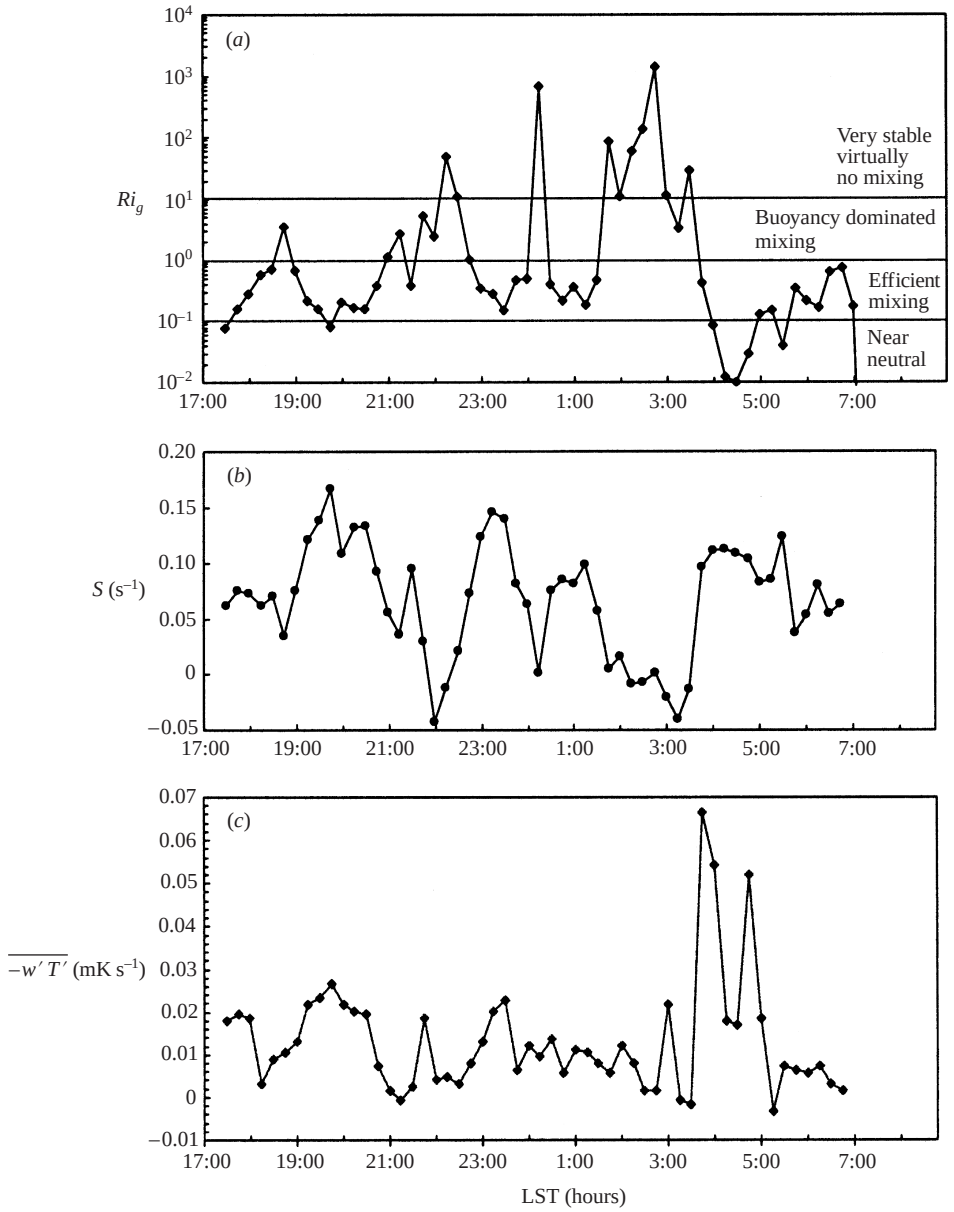

FIGURE 3. Nocturnal evolution of (*a*) Ri_g, (*b*) mean shear S (s^{-1}), and (*c*) heat flux $-\overline{w'T'}$ (mK s^{-1}) during a typical night at TA-6 (October 3, 2000).

and then a rapid decrease for $Ri_g > 1$. Note that Ri_g limits identified here are based on subjective judgment and have an uncertainty of $\pm 20\%$. The maximum mixing efficiency falls in the range $0.4 < R_f < 0.5$, consistent with the prediction of Townsend (1958) and the upper-bound estimate for turbulent Couette flows by Caulfield & Kerswell (2001). The Ri_g corresponding to the maximum mixing efficiency appears to be ~ 1. SF01*a* found that for $Ri_g < 1$ the vertical mixing is dominated by Kelvin–Helmholtz (KH) instabilities whereas internal wave breaking and Holmboe instabilities prevail for $Ri_g > 1$. Figure 1 clearly indicates that the Townsend (1958),

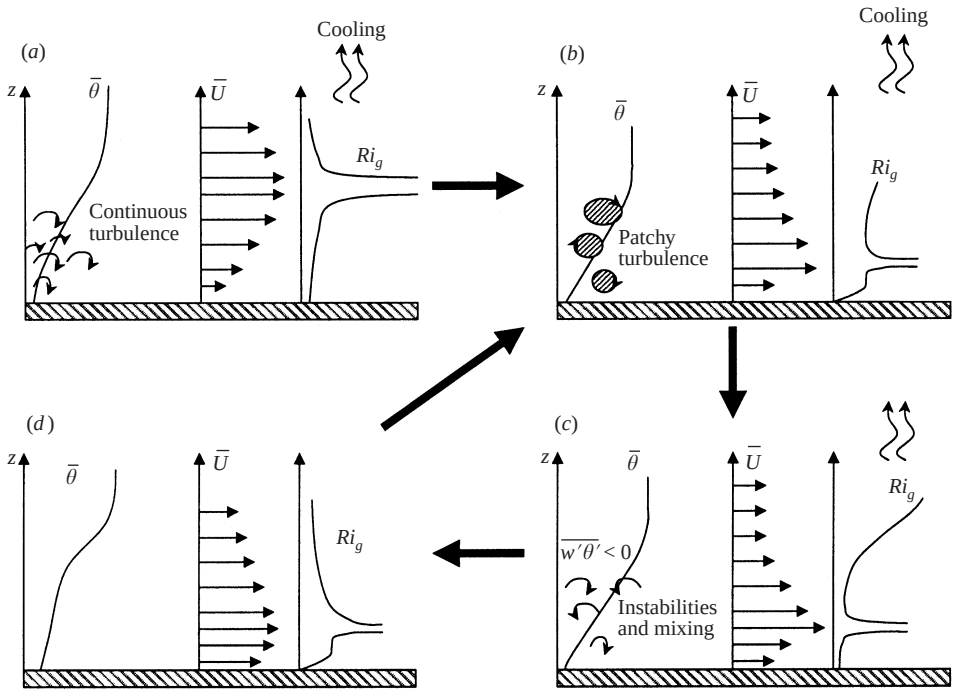

FIGURE 4. A schematic representation of the global intermittency cycle in the stable atmospheric boundary layer (not to scale).

MY82 and Nakanishi (2001) models fail for large $Ri_g(> 1)$. Tweaking of adjustable constants is needed if these models are to fit the data. For example, as shown in figure 1, the Townsend model, (1.7), shows better agreement with the $Ri_g < 1$ data when $\eta = 1/4$ is selected.

Based on figure 1, the descriptions of mixing mechanisms given by SF01*a* and the turbulent TKE production $P = -\overline{u_i' w'}\,\mathrm{d}\bar{U}_i/\mathrm{d}z$ and buoyancy flux $B = -(g/\Theta)\overline{w'T'}$ measurements (shown in figure 2), several flow regimes can be identified on the R_f–Ri_g plane. $Ri_g < 0.1$ is a 'near neutral' regime with low heat (or buoyancy) flux (characteristic of weak stratification) compared to shear production. For $0.1 < Ri_g < 1.0$, both P and B are comparable and mixing is efficient (which can be attributed to KH activity). Beyond $Ri_g \sim 1$, a fairly sharp levelling off of both P and B can be seen. Note that $1 < Ri_g < 10$ can be considered as a 'very stable' regime with low P and B, even though R_f therein is comparable to the 'efficient' mixing regime noted above. As discussed below, TKE budget measurements provide further information on long-time (on the order of hours) evolution of stable boundary layers.

Figure 3(*a*) shows the time evolution of Ri_g for a typical night at TA-6. Ri_g oscillates for several hours and then vanishes in the morning. The corresponding variations of shear S and heat flux $-\overline{w'T'}$ (or buoyancy flux) are shown in figures 3(*b*) and 3(*c*), respectively. The observed oscillatory behaviour is consistent with the 'global intermittency' of the nocturnal boundary layer advocated by Mahrt (1999) and is shown schematically in figure 4. Although the flat terrain case is illustrated for clarity, slope flows are also expected to behave similarly. Accordingly, in the early evening, the surface sensible heat flux becomes negative, causing stable stratification to develop and Ri_g to become positive resulting in a moderately stable boundary layer (figure 4*a*). With continuous cooling Ri_g increases and turbulence is suppressed further, thus

impeding vertical momentum transfer and confining turbulence to isolated patches (figure 4*b*). The lack of vertical momentum transfer causes shear to increase gradually, leading to a reduction of Ri_g until turbulence is re-generated (figure 4*c*), whence the shear drops and Ri_g increases again (figure 4*d*). The sequence of events (shown in figure 4*b*, *c*, *d*) continues until the stable stratification erodes away in the morning. This behaviour is evident in the measurements shown in figure 3, and is further discussed below.

Note that, as Ri_g increases through the 'efficient mixing' regime $0.1 < Ri_g < 1.0$, buoyancy effects become increasingly important, shear S remains the same or decreases (depending on vertical momentum transfer) and the flow sustains significant downward heat fluxes (B). When $Ri_g > 1$, vertical turbulent transport is impeded, thus enhancing vertical shear S between air layers. When the increase of S has an overriding influence, Ri_g begins to drop again, first through the 'efficient mixing' regime, wherein B is sustained, toward the 'neutral' regime, where B is relatively insignificant. In the latter regime, the vertical transport of momentum is effective and hence the shear drops substantially while Ri_g increases again, first through the 'efficient mixing' regime then into the very stable regime $Ri_g > 1$ whence shear rises again. As before, the buoyancy flux responds to these changes, sustaining up to $Ri_g \approx 10$ and essentially shutting off thereafter (see figure 2). The rising shear causes Ri_g to decrease again, with the fastest drops occurring in the proximity of the near-neutral regime whence the turbulence causes enhanced mixing, decrease of shear, followed by an increase in Ri_g. The sequence of events recurs over the night.

4. Conclusions

Turbulence data were obtained in two high-Reynolds-number stably stratified boundary layers on sloping terrain. These data were analysed to study the relationship between the flux (R_f) and gradient (Ri_g) Richardson numbers. One locale was a high desert Ponderosa pine forest in Los Alamos, New Mexico and the other was on the eastern slopes of Salt Lake City, Utah. Both were characterized by sloping terrain conducive to katabatic flows of characteristic Reynolds numbers (based on the boundary-layer thickness and mean speed) on the order of 10^7. The results indicated a consistent pattern of R_f–Ri_g variation, with R_f increasing with Ri_g at low Ri_g and decreasing at high Ri_g. The transition between the two regimes occurs at $Ri_g \sim 1$ where the maximum $R_f \sim 0.4$–0.5 occurs. The field results were in general agreement with laboratory data taken in a stratified shear layer by SF01*a*, *b*. This agreement suggests that the observed R_f–Ri_g trends may be interpreted in the light of the different mixing mechanisms delineated by SF01*a*, *b* for different Ri_g ranges. The buoyancy flux and the turbulent kinetic energy production showed distinct oscillations, consistent with the concept of global intermittency expounded by Mahrt (1999). Comparison of R_f–Ri_g data with the turbulent closure schemes of Townsend (1958), MY82 and Nakanishi (2001) indicate that, at larger $Ri_g > 1$, these models represent natural shear-induced mixing rather poorly.

This study was funded by DOE (Atmospheric Sciences Program, OBE), NSF (Fluid Mechanics and Atmospheric Sciences), and ARO (Geosciences). The authors wish to thank William Olson of ESH-17 at Los Alamos National Laboratory for his help in obtaining the TA-6 data set and Marko Princevac, Brian Chan and Thomas Kowalewski for their help in collecting the VTMX data.

REFERENCES

Baars, J., Holt, D. & Stone, G. 1998 Meteorological monitoring at Los Alamos. *LA-UR*-98-2148.

Caulfield, C. P. & Kerswell, R. R. 2001 Maximal mixing rate in turbulent stably stratified Couette flow. *Phys. Fluids* **13**, 894–900.

Caulfield, C. P. & Peltier, W. R. 2000 The anatomy of the mixing transition in homogeneous and stratified free shear layers. *J. Fluid Mech.* **413**, 1–47.

DeSilva, I. P. D., Brandt, A., Montenegro, L. J. & Fernando, H. J. S. 1999 Gradient Richardson number measurements in a stratified shear layer. *Dyn. Atmos. Oceans* **30**, 47–63.

Fornberg, B. 1996 *A Practical Guide to Pseudospectral Methods*. Cambridge University Press.

Ivey, G. N. & Imberger, J. 1991 On the nature of turbulence in a stratified fluid. Part 1: The energetics of mixing. *J. Phys. Oceanogr.* **21**, 650–658.

Lilly, D. K., Waco, D. E. & Adelfang, S. I. 1974 Stratospheric mixing estimated from high-altitude turbulence measurements. *J. Appl. Metl.* **13**, 488–493.

Linden, P. F. 1980 Mixing across a density interface produced by grid turbulence. *J. Fluid Mech.* **100**, 691–703.

Mahrt, L. 1982 Momentum balance of gravity flows. *J. Atmos. Sci.* **39**, 2701–2711.

Mahrt, L. 1999 Stratified atmospheric boundary layers. *Boundary-Layer Metl.* **90**, 375–396.

McEwan, A. D. 1983 Internal mixing in stratified fluids. *J. Fluid Mech.* **128**, 59–80.

Mellor, G. L. & Yamada T. 1982 Development of a turbulence closure model for geophysical fluid problems. *Rev. Geophys. Space Phys.* **20**, 851–875 (referred to as MY82 herein).

Monti, P., Fernando, H. J. S., Chan, W. C., Princevac, M., Kowalewski, T. A. & Pardyjak, E. 2002 Observations of flow and turbulence in the nocturnal boundary layer over a slope. *J. Atmos. Sci.* (in press).

Nakanishi, M. 2001 Improvement of the Mellor-Yamada turbulence closure model based on large-eddy simulation data. *Boundary-Layer Met.* **99**, 349–378.

Nieuwstadt, F. T. M. 1984 The turbulent structure of the stable, nocturnal boundary layer. *J. Atmos. Sci.* **41**, 2202–2216.

Oakey, N. S. 1982 Determination of the rate of dissipation of turbulent energy from simultaneous temperature and velocity shear microstructure measurements. *J. Phys. Oceanogr.* **12**, 256–271.

Osborn, T. R. 1980 Estimates of the local rate of vertical diffusion from dissipation measurements. *J. Phys. Oceanogr.* **10**, 83–89.

Phillips, O. M. 1972 Turbulence in a strongly stratified fluid – is it unstable? *Deep-Sea Res.* **19**, 79–81.

Posmentier, E. S. 1977 The generation of salinity finestructure by vertical diffusion. *J. Phys. Oceanogr.* **7**, 298–300.

Sorbjan, Z. 1986 On similarity in the atmospheric boundary layer. *Boundary-Layer Met.* **34**, 377–397.

Strang, E. J. & Fernando, H. J. S. 2001*a* Entrainment and mixing in stratified shear flows. *J. Fluid Mech.* **428**, 349–386 (referred to as SF01*a* herein).

Strang, E. J. & Fernando, H. J. S. 2001*b* Vertical mixing and transports through a stratified shear layer. *J. Phys. Oceanogr.* **31**, 2026–2048 (referred to as SF01*b* herein).

Stretch, D., Nomura, K. K. & Rottman, J. W. 2000 Mixing efficiency in decaying stably stratified turbulence. In *Fifth Intl Symp. on Stratified Flows*, Vol. II (ed. G. A. Lawrence, R. Pieters & N. Yonemitsu), pp. 1265–1268.

Townsend, A. A. 1958 The effects of radiative transfer on turbulent flow of a stratified fluid. *J. Fluid Mech.* **3**, 361–372.

Weinstock, J. 1978 Vertical turbulent diffusion in a stably stratified fluid. *J. Atmos. Sci.* **35**, 1022–1027.

Yamada, T. 1975 The critical Richardson number and the ratio of the eddy transport coefficients obtained from a turbulence closure model. *J. Atmos. Sci.* **32**, 926–933.